RESEARCH PAPER

Multi-material optimization design for mesh reflector antennas considering space thermal effects

Zihan Sun[1] · Baoyan Duan[1] · Yiqun Zhang[1] · Dongwu Yang[1] · Naigang Hu[1]

Abstract
Mesh reflector antennas are widely used in space missions, and the high requirements for reflector surface accuracy should be met to achieve reasonable electromagnetic performance. However, space-borne antennas usually experience periodic thermal loads, which deteriorate the reflector surface accuracy. Under these circumstances, this study carried out the thermal analysis and developed a multi-material optimization design approach for the cable-net structure of mesh reflector antennas considering space thermal effects. First, a mechanical analysis model of the cable-net structure is established, which can be used to calculate the nodal coordinates, cable forces, and surface accuracy under the influence of variable temperatures. Second, the complementary characteristics of different materials are used. The cable-net structure is made of multiple materials to minimize the variation range of on-orbit shape errors. Finally, numerical examples and ANSYS verification demonstrated that the proposed approach effectively improved the antenna's on-orbit surface accuracy. This work provides a new approach for mesh reflector antennas considering the on-orbit performances under thermal environments in space.

1 Introduction

With the rapid development of space technology, the requirements of large diameter, high precision, light weight, and high storage have been proposed for space-borne antennas. Deployable mesh reflector antennas have attracted more attention owing to their light weight and easy folding characteristics (Meguro and Harada 2003). Take the AstroMesh antenna shown in Fig. 1 as an example, it consists of a cable-net structure (including front net, rear net, and vertical cables), a supporting truss, and a wire mesh (Orikasa et al. 2013). The front net forms a paraboloid under the action of cable forces, and the wire mesh is attached to the front net to reflect electromagnetic waves. To meet the electromagnetic performance requirements, the antenna must have high surface accuracy (Ruze 1966; Hu et al. 2017; Cai and Feng 2015).

For a precise structure such as the space-borne antenna, the stability of the shape is one of the most important indexes after completing a high-precision design (Yang and Hou 2017; Zheng et al. 2022; Liu et al. 2019). Generally, the shape of the antenna is required to not fluctuate significantly with changes in the ambient temperature. However, space-borne antennas are periodically subjected to heat radiation from the sun with the movement of satellites; therefore, thermal stress and thermal deformation are generated in the antenna structure. Excessive thermal deformation directly affects the electromagnetic performance of the antenna and even causes thermal vibrations when entering and exiting the shadow area. According to previous research (Min 1991), the maximum thermal deformation of a 10 m aperture reflector antenna can reach 12 mm, while the root mean square (RMS) error of the reflector can reach 3.8 mm; the antenna gain will, therefore, be reduced by approximately 1.5 dB. Therefore, to ensure that the mesh reflector antenna has high thermal stability, it is necessary to conduct thermal analyses and ensure thermal control under a harsh space environment.
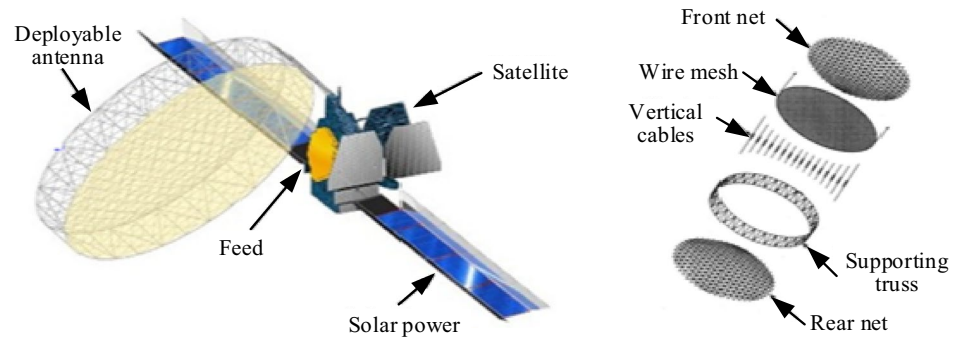
The current design methods are mainly divided into three categories: shape pre-design before launch, shape

---

Responsible Editor: Shikui Chen

✉ Yiqun Zhang
   yiqunzhang@xidian.edu.cn

[1] Key Laboratory of Electronic Equipment Structure Design
   of Ministry of Education, Xidian University, Xi'an 710071,
   Shaanxi, China

Fig. 1 AstroMesh antenna and its component

pre-adjustment before launch, and active shape adjustment on-orbit.

In the previous form-finding design, it is generally believed that, provided the cable-net structure has good tension uniformity, the mesh reflector antenna will possess good thermal stability. Therefore, the shape design of the cable-net structure is primarily aimed at tension uniformity. Morterolle et al. (Morterolle et al. 2012) proposed an equal-tension form-finding method to achieve a uniform tension distribution within an efficient zone. Considering that the boundary cable tensions vary over a large range, Yang et al. (Yang et al. 2018a) used the least-squares method to solve the boundary cable tensions under the premise that the cables within the efficient zone remain under uniform tension. Aiming at the asymmetric structure of the front and rear nets, Yang et al. (Yang et al. 2017) and Maddio et al. (Maddio et al. 2019) established a form-finding optimization model based on the force density method to ensure that the entire cable-net structure has good tension uniformity. However, the methods of ensuring thermal stability through tension uniformity do not fully consider the influence mechanism of the thermal environment on the cable-net structure, because the structural deformation caused by high/low temperatures is also related to the material properties and geometric configuration of the cable-net structure. By designing the cross-sectional area and tension of each cable element, Yang et al. (Yang et al. 2020) proposed a surface shape stability method, and the results showed that the reflector surface shape is insensitive to thermal loads. However, there exists a proportional relationship between the cross-sectional area of the cable element and its tension in this method. When the tensions are unevenly distributed, the cross-sectional area varies greatly, and engineering implementation is extremely difficult. Nie et al. (Nie et al. 2019) considered the influence of the space thermal effect in the form-finding design process and reduced the influence of the high/low temperature environment on the reflector surface accuracy by minimizing the maximum RMS error. By adjusting the antenna before launch to adapt it to the space temperature, Yang et al. (Yang et al. 2018b) established a pre-adjustment optimization model and solved the adjustment amount of the adjustable cables. Based on the design results, the core of the methods proposed by Nie

et al. (Nie et al. 2019) and Yang et al. (Yang et al. 2018b) is to modify the model to realize the translation of the surface accuracy curve in the temperature range, thus improving the worst surface accuracy; however, this does not actually solve the thermal stability problem. For example, the surface accuracies at some temperature conditions decreased.

With regard to active adjustment on-orbit, Tabata et al. (Tabata and Natori 1996) studied the feasibility of active shape correction under the conditions of a limited number of actuators and limited information on the surface shape. Wang et al. (Wang et al. 2013) and Xun et al. (Xun et al. 2018) conducted an active shape adjustment of the cable-net structure by incorporating piezoelectric (PZT) actuators into flexible cables. These studies have also achieved ideal results in theory. However, the lack of necessary on-orbit measurement capabilities and the complexity of the active adjustment system limit the application of these methods.

Therefore, to alleviate the influence of the space thermal loads on the reflector surface accuracy, this study considers the complementary characteristics of different materials and plans to use multiple materials to manufacture the cable-net structure. The remainder of this paper is organized as follows. Based on the finite element analysis, the mechanical model of the cable-net structure of the mesh reflector antenna is established in Sect. 2, and the expressions of the nodal positions, cable forces, and surface accuracy under the influence of ambient temperature are derived. In Sect. 3, a multi-material optimization design model considering space thermal effects is established, and the solution strategy is presented based on the genetic algorithm. Section 4 demonstrates the effectiveness of the proposed approach through case studies. Finally, the conclusions and discussions are summarized in Sect. 5.

2 Mechanical model considering space thermal effects

After completing the form-finding design of cable-net structure of the mesh reflector antenna, the next step is to select optimal materials to manufacture it. In this study, we assume that two materials are used to manufacture the cable-net
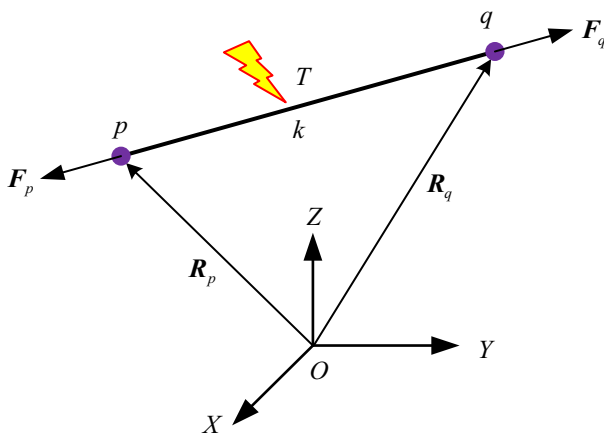
Fig. 2 Space cable element in equilibrium state

structure. The elastic modulus, cross-sectional area, and thermal expansion coefficient of the first material are $E^{(1)}$, $A^{(1)}$, and $\alpha^{(1)}$, respectively. The elastic modulus, cross-sectional area, and thermal expansion coefficient of the second material are $E^{(2)}$, $A^{(2)}$, and $\alpha^{(2)}$, respectively. When a material is randomly selected to fabricate the cable element k, its material properties can be expressed as:

$$\begin{cases} E_k = \beta_k E^{(1)} + (1 - \beta_k) E^{(2)} \\ A_k = \beta_k A^{(1)} + (1 - \beta_k) A^{(2)} \\ \alpha_k = \beta_k \alpha^{(1)} + (1 - \beta_k) \alpha^{(2)} \end{cases} \tag{1}$$

in which

$$\beta_k = \{1, 0\} \tag{2}$$

where $\beta_k = 1$ indicates that the k-th cable element is fabricated by the first material, and $\beta_k = 0$ indicates that the k-th cable element is fabricated by the second material.

Consider a space cable element k in an equilibrium state with the nodes p and q, as shown in Fig. 2 (Du et al. 2013; Sun et al. 2021). Neglecting the influence of space microgravity, only the initial pre-stress and space thermal stress were considered. According to Hooke's law, the nodal force $\boldsymbol{F}_p$ can be calculated as

$$\boldsymbol{F}_p = E_k A_k \left(\varepsilon_k^F - \varepsilon_k^T \right) \cdot \boldsymbol{n}_k \tag{3}$$

where ε_k^F is the strain generated by the cable element k under the action of pretension F, that is,

$$\varepsilon_k^F = \frac{L_k - L_{0,k}}{L_{0,k}} \tag{4}$$

ε_k^T is the strain produced by the cable element k under the influence of temperature T, that is,

$$\varepsilon_k^T = \alpha_k (T - T_0) \tag{5}$$

$\boldsymbol{n}_k$ is the unit vector of the cable element k, which is defined as pointing from node q to node p, that is,

$$\boldsymbol{n}_k = \frac{\boldsymbol{R}_p - \boldsymbol{R}_q}{L_k} \tag{6}$$

T_0 is the ambient temperature of cable element k without thermal deformation; $L_{0,k}$ is the unstressed length of cable element k; L_k is the length of cable element k after applying pretension, that is,

$$L_k = \left[\left(\boldsymbol{R}_p - \boldsymbol{R}_q \right)^{\mathrm{T}} \left(\boldsymbol{R}_p - \boldsymbol{R}_q \right) \right]^{1/2} \tag{7}$$

The nodal force $\boldsymbol{F}_p$ can be expressed as a function of the relative nodal position, $\boldsymbol{R}_p - \boldsymbol{R}_q$, and the ambient temperature, T, as follows:

$$\boldsymbol{F}_p = \mathbf{F}(\boldsymbol{R}_p - \boldsymbol{R}_q, T) \tag{8}$$

When the variation in the ambient temperature is small, the large displacement characteristics of the cable-net structure cannot be considered. By neglecting the higher-order terms, the first-order Taylor expansion of Eq. (8) is obtained as follows:

$$\Delta \boldsymbol{F}_p = \boldsymbol{k}_{ck} (\Delta \boldsymbol{R}_p - \Delta \boldsymbol{R}_q) + \boldsymbol{k}_{tk} \Delta T \tag{9}$$

where

$$\begin{aligned} \boldsymbol{k}_{ck} &= \frac{\partial \boldsymbol{F}_p}{\partial (\boldsymbol{R}_p - \boldsymbol{R}_q)} \\ &= E_k A_k \left(\frac{1}{L_{0,k}} - \frac{1}{L_k} (1 + \alpha_k (T - T_0)) \right) \boldsymbol{I}_3 + \frac{E_k A_k (1 + \alpha_k (T - T_0))}{L_k^3} (\boldsymbol{R}_p - \boldsymbol{R}_q)(\boldsymbol{R}_p - \boldsymbol{R}_q)^{\mathrm{T}} \end{aligned} \tag{10}$$

$$k_{tk} = \frac{\partial \mathbf{F}_p}{\partial T} = -\frac{E_k A_k \alpha_k}{L_k}(\mathbf{R}_p - \mathbf{R}_q) \qquad (11)$$

and $\mathbf{I}_3$ is a 3×3 identity matrix.

Noting that cable element k is in equilibrium, i.e.,

$$\Delta \mathbf{F}_q = -\Delta \mathbf{F}_p \qquad (12)$$

By combining Eqs. (9) and (12), the incremental relationship of the cable element k can be expressed as

$$\begin{bmatrix} \Delta \mathbf{F}_p \\ \Delta \mathbf{F}_q \end{bmatrix} = \begin{bmatrix} k_{ck} & -k_{ck} \\ -k_{ck} & k_{ck} \end{bmatrix} \begin{bmatrix} \Delta \mathbf{R}_p \\ \Delta \mathbf{R}_q \end{bmatrix} + \begin{bmatrix} k_{tk} \\ -k_{tk} \end{bmatrix} \Delta T \qquad (13)$$

Based on the topological connection between the cable elements, the incremental equilibrium equation of the cable-net structure can be assembled and expressed as:

$$\Delta \mathbf{F} = \mathbf{K}_c \Delta \mathbf{R} + \mathbf{K}_t \Delta T \qquad (14)$$

2.1 Incremental displacement equation

Referring to classification into free and boundary nodes, as illustrated in Fig. 3, the incremental equilibrium equation is expressed in blocks as follows:

$$\begin{bmatrix} \Delta \mathbf{F}_f \\ \Delta \mathbf{F}_b \end{bmatrix} = \begin{bmatrix} \mathbf{K}_c^{11} & \mathbf{K}_c^{12} \\ \mathbf{K}_c^{21} & \mathbf{K}_c^{22} \end{bmatrix} \begin{bmatrix} \Delta \mathbf{R}_f \\ \Delta \mathbf{R}_b \end{bmatrix} + \begin{bmatrix} \mathbf{K}_t^1 \\ \mathbf{K}_t^2 \end{bmatrix} \Delta T \qquad (15)$$

where $\Delta \mathbf{F}_f$ and $\Delta \mathbf{F}_b$ are the incremental external forces of the free and boundary nodes, respectively; $\Delta \mathbf{R}_f$ and $\Delta \mathbf{R}_b$ are the incremental nodal displacements of the free and boundary nodes, respectively; $\mathbf{K}_c^{11}$, $\mathbf{K}_c^{12}$, $\mathbf{K}_c^{21}$ and $\mathbf{K}_c^{22}$ are the partitioned

● Free nodes   ● Boundary nodes
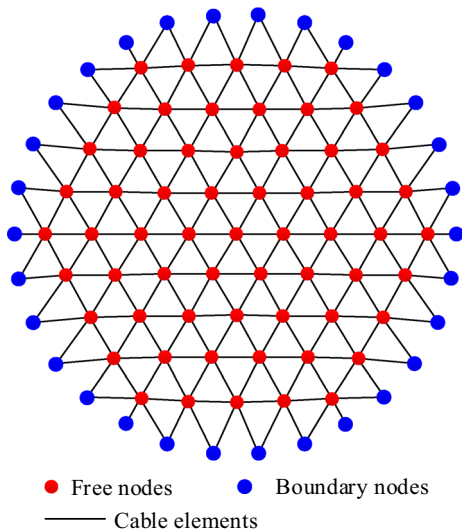—— Cable elements

Fig. 3 Classification of cable-net nodes

matrices of matrix $\mathbf{K}_c$ after rearrangement; and $\mathbf{K}_t^1$ and $\mathbf{K}_t^2$ are the partitioned matrices of matrix $\mathbf{K}_t$ after rearrangement.

Temperature can be regarded as a factor that affects the internal tension of the cable elements, and it is not an external load (Yang et al. 2018b). Thus, there is no external force, i.e., $\Delta \mathbf{F}_f = \mathbf{0}$; and the deformation of supporting truss is not considered, i.e., $\Delta \mathbf{R}_b = \mathbf{0}$. Substituting these into Eq. (15) leads to the relationship between the displacements of free nodes and the variation in temperature, as follows:

$$\Delta \mathbf{R}_f = \mathbf{K}_{ct} \Delta T \qquad (16)$$

where $\mathbf{K}_{ct} = -\left(\mathbf{K}_c^{11}\right)^{-1} \mathbf{K}_t^1$ is the sensitivity matrix of the nodal displacements with respect to temperature variation.

Therefore, under the influence of ambient temperature T, the nodal coordinates of the cable-net structure can be obtained as

$$\mathbf{R}(T) = \mathbf{R}(T_0) + \Delta \mathbf{R} \qquad (17)$$

where $\mathbf{R}(T_0)$ represent the nodal coordinates at the ambient temperature T_0.

2.2 Incremental force equation

From the Eq. (9), the incremental forces of the cable element k is expressed as:

$$\Delta \mathbf{F}_k = \Delta \mathbf{F}_p = k_{ck}(\Delta \mathbf{R}_p - \Delta \mathbf{R}_q) + k_{tk}\Delta T \qquad (18)$$

According to the topological relationship, the incremental force equations of all cable elements are written in matrix form as follows:

$$\Delta \mathbf{F}^F = \mathbf{K}_c^F (\mathbf{C} \otimes \mathbf{I}_3)\Delta \mathbf{R} + \mathbf{K}_t^F \Delta T \qquad (19)$$

where $\mathbf{K}_c^F = \mathrm{diag}(k_{c1}, k_{c2}, \cdots, k_{cm})$ and $\mathbf{K}_t^F = \mathrm{diag}(k_{t1}, k_{t2}, \cdots, k_{tm})$; diag($\cdot$) stands for block diagonal matrix, $\otimes$ represents tensor product, and $\mathbf{C}$ is the topology matrix of the cable-net structure defined in the field of graph theory (Kaveh 2004), which can be written as

$$\mathbf{C}(k, v) = \begin{cases} 1, & v = p \\ -1, & v = q \\ 0, & \text{otherwise} \end{cases} \qquad (20)$$

where $k(k = 1 \sim m)$ is the number of cable elements, $v(v = 1 \sim n)$ is the number of cable-net nodes, m is the total number of cable elements, and n is the total number of cable-net nodes.

The incremental forces in the axial direction of all cable elements can be calculated as

$$\Delta \mathbf{F}_a = \mathbf{N}\Delta \mathbf{F}^F \qquad (21)$$

where $N = \text{diag}\left(n_1^{\text{T}}, n_2^{\text{T}}, \cdots, n_m^{\text{T}}\right)$.

Therefore, under the influence of ambient temperature T, the cable forces of the cable-net structure can be obtained as

$$F_a(T) = F_a(T_0) + \Delta F_a \tag{22}$$

where $F_a(T_0)$ represent the cable forces at the ambient temperature T_0.

2.3 Surface accuracy analysis

For mesh reflector antennas, the nodal deviation between the deformed reflector and the desired paraboloid can efficiently reflect the deviation extent of the former from the latter (Sun et al. 2021). Therefore, the RMS deviation between the deformed reflector and the desired paraboloid is typically used to describe the surface accuracy of the antenna.

The wire mesh is attached to the front net to form a working reflective surface; therefore, it is only necessary to ensure that the free nodes of the front net are located on the desired paraboloid to the maximum extent. Equation (16) is divided into blocks, as follows:

$$\begin{bmatrix} \Delta R_f^{\text{f}} \\ \Delta R_f^{\text{r}} \end{bmatrix} = \begin{bmatrix} K_{\text{ct}}^{\text{f}} \\ K_{\text{ct}}^{\text{r}} \end{bmatrix} \Delta T \tag{23}$$

where ΔR_f^{f} and ΔR_f^{r} represent the incremental displacements of the free nodes of the front and rear nets, respectively; and K_{ct}^{f} and K_{ct}^{r} are the corresponding matrices.

From the Eq. (23), the incremental displacements of the free nodes of the front net can be obtained as

$$\Delta R_f^{\text{f}} = K_{\text{ct}}^{\text{f}} \Delta T \tag{24}$$

The free nodes of the front net are denoted by set Q, and the number of nodes by Nup. The divergence of an arbitrary node $i(i \in Q)$ with respect to the desired paraboloid is calculated as follows:

$$\begin{aligned} \delta_i &= \frac{x_i^2 + y_i^2}{4F_p} - z_i \\ &= \frac{\left(x_{0i} + \Delta x_i\right)^2 + \left(y_{0i} + \Delta y_i\right)^2}{4F_p} - \left(z_{0i} + \Delta z_i\right) \end{aligned} \tag{25}$$

where $\begin{bmatrix} x_0 & y_0 & z_0 \end{bmatrix}^{\text{T}}$ represent the coordinate vectors of the free nodes of the front net at the ambient temperature T_0, and F_p is the focal length of the desired paraboloid.

Because the divergence between the deformed reflector and the desired paraboloid is very small during a small change in temperature, the second-order terms of the displacement in Eq. (25) can be omitted. Thus, Eq. (25) can be simplified as follows:

$$\begin{aligned} \delta_i &= \frac{x_{0i}}{2F_p}\Delta x_i + \frac{y_{0i}}{2F_p}\Delta y_i - \Delta z_i + \frac{x_{0i}^2 + y_{0i}^2}{4F_p} - z_{0i} \\ &= A_i \Delta R_{fi}^{\text{f}} + b_i \end{aligned} \tag{26}$$

where $A_i = \begin{bmatrix} x_{0i}/2F_p & y_{0i}/2F_p & -1 \end{bmatrix}$, $\Delta R_{fi}^{\text{f}} = \begin{bmatrix} \Delta x_i & \Delta y_i & \Delta z_i \end{bmatrix}^{\text{T}}$, $b_i = \left(x_{0i}^2 + y_{0i}^2\right)/4F_p - z_{0i}$.

The sum of the squares of the z-direction deviations of all nodes on the reflecting surface can be expressed as

$$\begin{aligned} f(T) &= \sum_{i \in Q} \delta_i^2 = \sum_{i \in Q} \left(A_i \Delta R_{fi}^{\text{f}} + b_i\right)^2 \\ &= \left(\Delta R_f^{\text{f}}\right)^{\text{T}} A^{\text{T}} A \Delta R_f^{\text{f}} + 2B^{\text{T}} A \Delta R_f^{\text{f}} + B^{\text{T}} B \end{aligned} \tag{27}$$

where $A = \text{diag}\left(\begin{bmatrix} A_1 & A_2 & \cdots & A_{Nup} \end{bmatrix}\right)$ and $B = \begin{bmatrix} b_1 & b_2 & \cdots & b_{Nup} \end{bmatrix}^{\text{T}}$.

Substituting Eq. (24) into Eq. (27), it can be calculated as

$$\begin{aligned} f(T) &= \left(K_{\text{ct}}^{\text{f}} \Delta T\right)^{\text{T}} A^{\text{T}} A \left(K_{\text{ct}}^{\text{f}} \Delta T\right) + 2B^{\text{T}} A \left(K_{\text{ct}}^{\text{f}} \Delta T\right) + B^{\text{T}} B \\ &= (\Delta T)^{\text{T}} A_c \Delta T + 2B_c^{\text{T}} \Delta T + C_c \end{aligned} \tag{28}$$

where $A_c = \left(AK_{\text{ct}}^{\text{f}}\right)^{\text{T}} AK_{\text{ct}}^{\text{f}}$, $B_c = AK_{\text{ct}}^{\text{f}} B$, $C_c = B^{\text{T}} B$.

Therefore, under the influence of ambient temperature T, the surface accuracy of the mesh reflector antenna can be obtained as

$$\text{RMS}(T) = \sqrt{\frac{f(T)}{Nup}} \tag{29}$$

3 Optimization design with multiple materials

3.1 Optimization model

In the derivation process of the incremental equilibrium equation in Sect. 2, it is assumed that the temperature variation is small; thus, the linearization method is used to analyze the mechanical model of the cable-net structure. However, the cable-net structure is a geometrically nonlinear structure. If the ambient temperature varies significantly, direct linearization will inevitably lead to large deviations. Therefore, this study adopts the step-by-step linearization analysis method to consider the geometric nonlinearity. Treat the space temperature as an interval variable denoted by $T \in [T_{\min}, T_{\max}]$, and divide the temperature interval into several steps according to the step size ΔT, such as $[T_1, T_2, \cdots, T_t]$. First, nodal coordinates and cable forces at ambient temperature T_0, which are obtained by form-finding design, can be taken as the initial values to establish the incremental equilibrium equation of the cable-net structure and solve the equilibrium state at temperature $\left(T_0 \pm \Delta T\right)$.

Then, the nodal coordinates and cable forces at temperature $(T_0 \pm \Delta T)$ are taken as the initial values to solve the equilibrium state at the next temperature step. The process was repeated until the temperature reached its maximum and minimum values. Therefore, if the nodal coordinates and cable forces at ambient temperature T_0 are prescribed by the form-finding design, the equilibrium states and RMS errors at other temperatures can be solved.

Above all, the material optimization design model of the cable-net structure, considering the space thermal effects, can be conducted. Take the material types of the cable elements as the design variables, the cable forces as the constraint condition, and the maximum value of the RMS errors at all temperature steps as the optimization objective. The established optimization model is as follows:

$$
\begin{aligned}
&\text{Find}\quad \boldsymbol{\beta} = \begin{bmatrix} \beta_1 & \beta_2 & \cdots & \beta_m \end{bmatrix}^{\mathrm{T}} \\
&\text{Min}\quad \max\left\{ \mathrm{RMS}(T_1)\ \mathrm{RMS}(T_2)\ \cdots\ \mathrm{RMS}(T_t) \right\} \quad (30) \\
&\text{S.t.}\quad F_{ak} > 0, \quad k = 1, 2, \cdots, m
\end{aligned}
$$

where t is the number of temperature steps; and F_{ak} is the force of the cable element k, which is required to be a positive value to ensure that the cable element does not slack.

3.2 Solution strategy

Considering that this optimization model is a typical highly nonlinear problem, it is difficult to obtain the sensitivity information of the objective function and design variables; therefore, the genetic algorithm is used to solve it (Bao and Yu 2017). The solution process is described as follows. First, an initial binary population is created, and the fitness of each individual in the population is calculated. Then, it is determined whether the iteration termination condition is met. If they are satisfied, the iteration ends and the optimal individual as the optimization result is output; otherwise, the genetic operations of selection, crossover, and mutation are performed on the individuals in the population. For the filial generation, the termination criterion is determined again, and the iteration continues until the termination condition is satisfied. The optimization design procedure is illustrated in Fig. 4.

(1) Coding operation The binary parameter vectors whose number of individuals is *NP* and the dimension of each individual is *m* are used as a population, in which each individual is expressed as:

$$
\boldsymbol{h}_{j,\mathrm{g}}(j = 1, 2, \cdots, NP) \tag{31}
$$

Fig. 4 Flow chart of the proposed approach
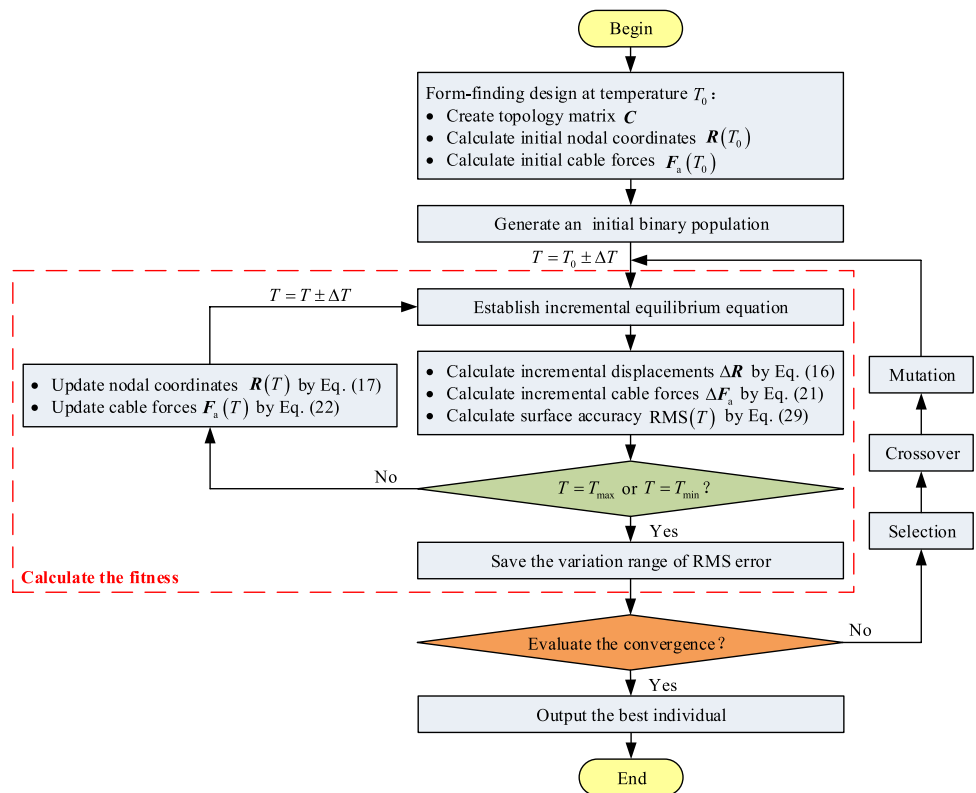
where j represents the sequence number of the individual in the corresponding population, and g represents the evolutionary generation.

Then, individuals of the population must initially be coded to establish the starting points for optimization. Assuming that initialized individuals obey a random uniform distribution, the initial value of the j-th individual can be obtained by:

$$h_{j,0} = \text{randint}(1, m) \tag{32}$$

where $\text{randint}(1, m)$ is used to generate a vector of length m, and the elements in the vector are randomly selected to be 0 or 1.

(2) Selection operation Using the "roulette" selection method, the proportion of each individual's fitness is used to determine the possibility that it will be retained. If the fitness of an individual is fit_j, the probability of it being selected can be calculated as

$$P_{sj} = fit_j \bigg/ \sum_{j=1}^{NP} fit_j \tag{33}$$

in which fit_j can be described by the maximum value of the RMS errors at all temperature steps and obtained after normalization as follows:

$$fit_j = \frac{\text{RMS}_{\text{max},j} - \min\left(\mathbf{RMS}_{\text{max}}\right)}{\max\left(\mathbf{RMS}_{\text{max}}\right) - \min\left(\mathbf{RMS}_{\text{max}}\right)} \tag{34}$$

where $\mathbf{RMS}_{\text{max}}$ represents the set consisting of the maximum RMS errors corresponding to all individuals, that is,

$$\mathbf{RMS}_{\text{max}} = \begin{bmatrix} \text{RMS}_{\text{max},1} & \text{RMS}_{\text{max},2} & \cdots & \text{RMS}_{\text{max},NP} \end{bmatrix} \tag{35}$$

and $\text{RMS}_{\text{max},j}$ is the maximum RMS error of the j-th individual in the temperature interval, i.e.,

$$\text{RMS}_{\text{max},j} = \max\left\{ \text{RMS}(T_1) \ \text{RMS}(T_2) \ \cdots \ \text{RMS}(T_t) \right\} \tag{36}$$

For this problem, the smaller the maximum value of the RMS error in the temperature range, the better the fitness of the individual and the greater the chance of being selected. A random number r_s is generated in the interval [0, 1] in each round of selection. If $P_{sj} < r_s$, the current individual is retained; otherwise, it is discarded. Finally, to ensure that the number of population remains unchanged, multiple rounds of selection are required.

(3) Crossover operation Match the selected odd-numbered individual $\boldsymbol{h}_{2j-1,g}$ and even-numbered individual $\boldsymbol{h}_{2j,g}$. For each pair of individuals, some of the genes between them are exchanged with crossover probability P_c. The crossover operation is as follows: first, take out a pair of individuals to be mated; then, randomly select the integers in the pair of individuals as the crossover positions; finally, generate a random number r_c in the interval [0, 1]. If $r_c < P_c$, the selected paired individuals exchange part of their genes at the crossover positions, thus forming a new pair of individuals.

(4) Mutation operation For each individual in the population, the gene value of some loci changes with the mutation probability P_m to the value of other alleles. The mutation operation is as follows: first, select the j-th individual in the population after completing the crossover operation, then a random number r_m is generated in the interval [0, 1] and some integers are randomly selected in the interval $[1, m]$ as the mutation positions. If $r_m < P_m$, the gene at this position is selected as the mutation gene, and its value is changed to the opposite value.

4 Case studies

According to previous experiments and numerical simulations (Foster and Aglietti 2010), the temperature of spaceborne antennas ranges from approximately – 200 to 100 °C. Therefore, the temperature interval is set to $T \in [-200, 100]$ °C. Correspondingly, the temperature at which the material does not undergo thermal deformation is generally assumed to be 20 °C. Considering the better translucency of the mesh reflector antenna and ignoring the shielding effect of the antenna structure, it is assumed that the temperature distribution of the antenna is uniform, and its value varies within an interval. If the non-uniform temperature distribution of the antenna at different orbital positions can be determined, Multi-material optimization design can also be conducted by modifying the cable element's temperature from a uniform value to a set of temperature values (Nie et al. 2019).

Taking a 10 m aperture mesh reflector antenna as an example, the focal length of the front net is 8 m, and the cable-net structure is shown in Fig. 5 after completing the form-finding design (Yang et al. 2016). Considering that Kevlar and carbon fiber are commonly used in space, this study uses these two materials to manufacture the cable elements of the cable-net structure. The corresponding material parameters are presented in Table 1.

In the genetic algorithm, the number of populations was set to 50, the crossover rate was 0.85, the mutation rate was 0.05, and the maximum generation was 100. The CPU adopted for optimization is Intel(R) Core(TM) i5-6500 at 3.20 GHz with 8.00 GB RAM, and the runtime per generation is about 67 s. The optimization results obtained under different initial populations are shown in Fig. 6 and Table 2. It can be seen that since the initial populations are
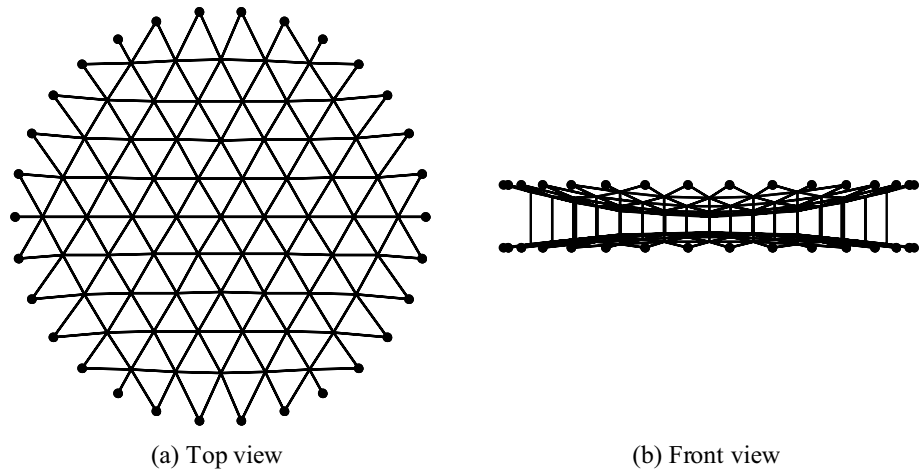
Fig. 5 Cable-net structure model

(a) Top view   (b) Front view

Table 1 Parameters of two materials

Item	Material one	Material two
Name	Kevlar	Carbon fiber (T300)
Elastic modulus (GPa)	20	80
Cross-sectional area (mm^2)	0.785	0.785
Thermal expansion coefficient (°C^{-1})	-2×10^{-6}	2×10^{-6}

Table 2 Optimization results with different initial populations

Item	CPU time (s)	RMS error at temperature (mm)	
		-200 °C	100 °C
Case one	6636.72	1.5920	0.6078
Case two	6578.68	1.5392	0.6252
Case three	6700.38	1.4918	0.5646
Case four	6766.26	1.6550	0.6288
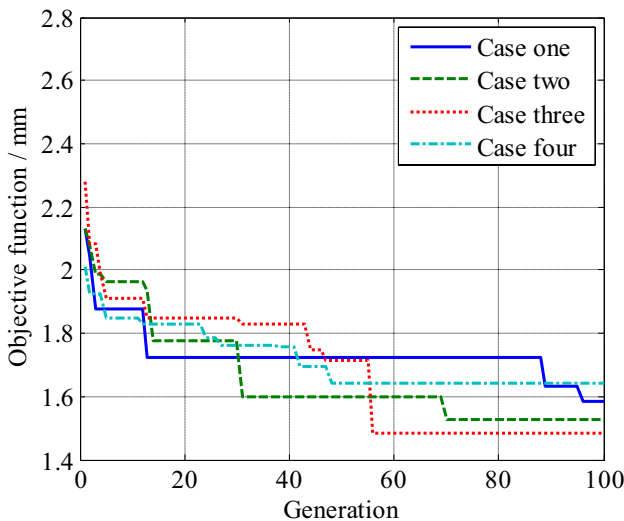
Fig. 6 Iterative histories with different initial populations

randomly generated, the optimization results are different. For explanation, the optimal result (Case three) is selected to demonstrate the effectiveness of the proposed approach. The material distribution of the cable elements is shown in Fig. 7, where the blue solid line indicates that the cable element uses Kevlar material, and the red dotted line indicates that the cable element uses carbon fiber material.

In Fig. 8, the results using only the Kevlar material are indicated by the black curve marked by the squares, the results using only the carbon fiber material are represented by the blue curve marked by the rhombuses, and the results of the proposed approach are denoted by the red curve marked by the circles. The RMS error is reduced from 2.93 mm (using Kevlar material) and 3.05 mm (using carbon fiber material) to 1.49 mm at -200 °C; the RMS error is reduced from 1.03 mm (using Kevlar material) and 1.15 mm (using carbon fiber material) to 0.56 mm at 100 °C. The maximum value of the RMS error in the temperature range was reduced by 49.15% (using Kevlar material) and 51.15% (using carbon fiber material). Therefore, compared to choosing only one material (Kevlar or carbon fiber) in the traditional manufacturing process of the cable-net structure, the reflector surface accuracy over the entire temperature range is significantly improved by reasonably choosing the material type of each cable element.

Meanwhile, as shown in Fig. 9, the results designed in this study are compared with the results calculated by the method mentioned in Ref. (Nie et al. 2019), which are expressed by the brown curve marked by the cross. Compared to the method mentioned in Ref. (Nie et al. 2019), the method proposed in this study achieves a reduction in the RMS error under all conditions in the temperature range, and the magnitude of the decline is greater (under the condition

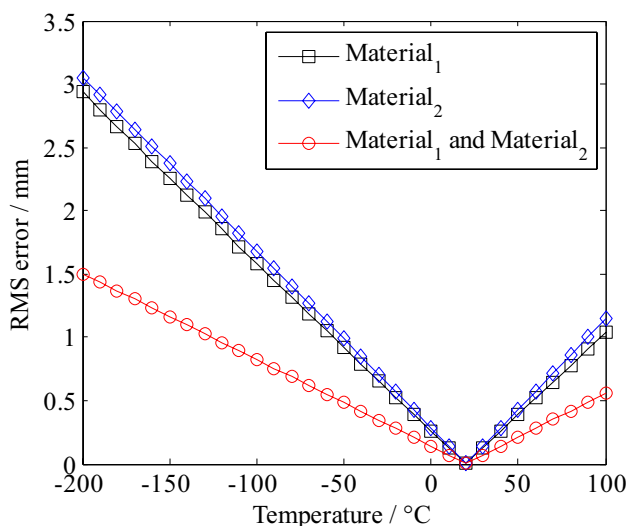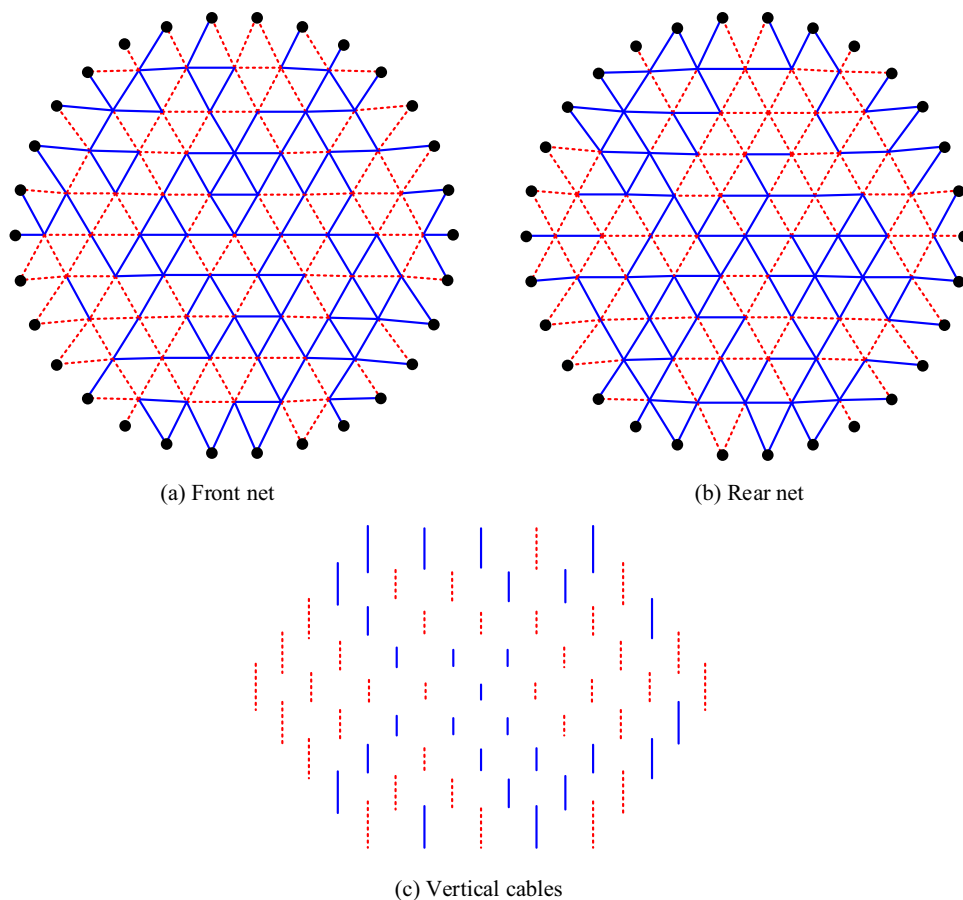**Fig. 7** Material distribution of cable-net structure

(a) Front net

(b) Rear net

(c) Vertical cables

Fig. 8 Distribution of RMS errors

Fig. 9 Comparison of the RMS errors

of −200 °C, the method mentioned in Ref. (Nie et al. 2019) reduces the RMS error from 2.93 to 2.01 mm, which is a reduction of 31.40%.
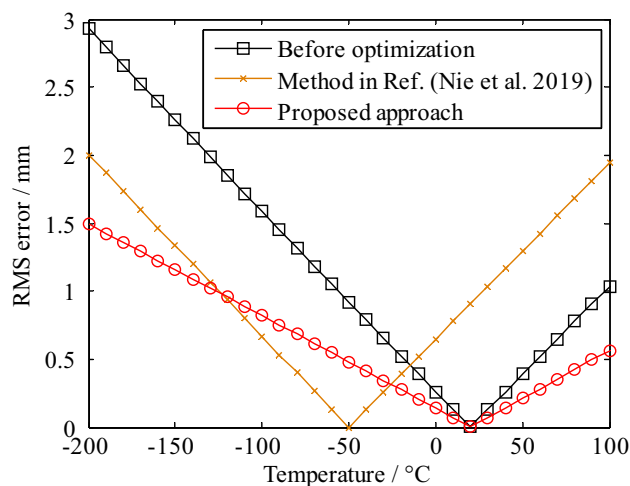
Finally, to verify the proposed approach, the design results are substituted into the commercial software ANSYS (version 15.0) to calculate the RMS errors under all conditions in the temperature range. In Fig. 10, the maximum deviation
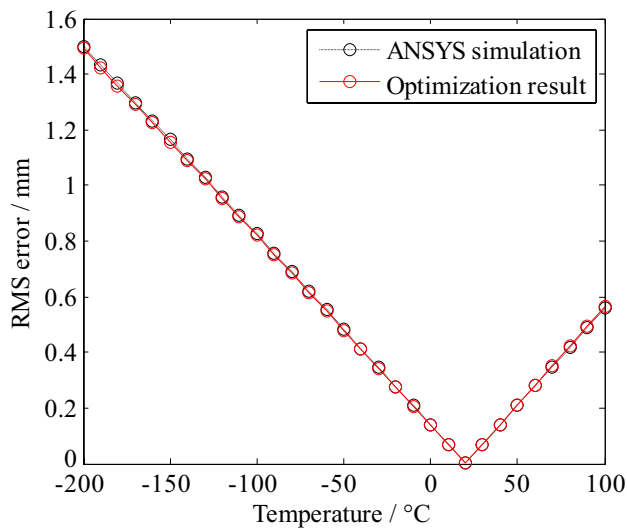
Fig. 10 Result verification

Table 3 Optimization results with different generations

Generation	CPU runtime (s)	RMS error at temperature (mm)	
		$-200\ °C$	$100\ °C$
100	6700.38	1.4918	0.5646
300	20,341.02	1.4310	0.5533
500	33,979.83	1.4101	0.5433

between the RMS errors obtained by the ANSYS simulation and the proposed approach is 0.009 mm at $-200\ °C$. Compared to the value of the RMS error at this temperature, the deviation ratio is 0.6%, which is an acceptable deviation.

It is worth noting that this study uses the genetic algorithm to solve the optimization model, and the current result is obtained after only 100 generations of evolution. It is well known that using a random search method to optimize the solution, the possibility of obtaining the global optimal solution increases with the number of evolutions. As shown in Table 3, with the increase of the evolutionary generations, better optimization results are found, but obviously the time also increases. Therefore, if it is necessary to further reduce the RMS error in the temperature range, it can be achieved by increasing the evolutionary generation, but this will increase the time taken by the population to continue to evolve.

5 Conclusions

In this study, the thermal analysis and thermal control of a space-borne mesh reflector antenna under an extreme thermal environment were carried out. Considering that the

preliminary adjustment before launch is limited by the number of adjustable cables, and the active adjustment on-orbit is still in the theoretical research stage, this study utilizes the complementary characteristics of different materials and adopts multiple materials to manufacture the cable-net structure of the mesh reflector antenna. In this manner, the variation range of the on-orbit surface error of the mesh reflector antenna is narrowed, and the worst surface shape is also improved. Numerical examples are provided to demonstrate the necessity and effectiveness of the proposed approach. Simultaneously, the obtained results matched well with the ANSYS simulation. Certain key points can be drawn as follows:

(1) From the expressions of nodal coordinates, cable forces, and surface accuracy, it can be seen that the structural deformation caused by the thermal environment is closely related to the tension distribution, material properties, and geometric configuration of the cable-net structure.
(2) By changing the material distribution of the cable-net structure, the sensitivity of the nodal displacements with respect to the temperature variation is reduced, and the thermal stability of the cable-net structure is also improved.

Finally, owing to the limitations of knowledge and time, there is still much work that has not been carried out. For example, not only the cable-net structure with a large thermal expansion coefficient will be affected by the thermal environment, but also the supporting truss made of high elastic modulus material will undergo thermal deformation. In previous research, we paid more attention to the deployment characteristics of the supporting truss; hence, thermal deformation was not considered. In the future, to achieve higher precision of the mesh reflector antenna under the space thermal environment, the cable-net structure, wire mesh, and supporting truss should be designed and analyzed in an integrated form to ensure the high thermal stability of the antenna.

Declarations

Conflict of interest The authors declare that they have no known competing financial interests or personal relationships that could have appeared to influence the work reported in this paper.

Replication of results The results presented in this study can be replicated by implementing the formulas and data structures presented in

this study. The code and data for producing the presented results will be made available by request.

References

Bao ZY, Yu JZ (2017) Genetic algorithm based on MATLAB and its application in sparse array antenna. Publishing House of Electronics Industry, Beijing (**In Chinese**)

Cai JG, Feng J (2015) Form-finding of tensegrity structures using an optimization method. Eng Struct 104:126–132

Du JL, Zong YL, Bao H (2013) Shape adjustment of cable mesh antennas using sequential quadratic programming. Aerosp Sci Technol 30(1):26–32

Foster JA, Aglietti GS (2010) The thermal environment encountered in space by a multifunctional solar array. Aerosp Sci Technol 14:213–219

Hu NG, Bao H, Duan BY et al (2017) Topology optimization of reflector antennas based on integrated thermal-structural-electromagnetic analysis. Struct Multidisc Optim 55:715–722

Kaveh A (2004) Structural Mechanics: Graph and matrix methods, 3rd edn. Research Studies Press, Somerset, UK

Liu RW, Guo HW, Liu RQ et al (2019) Design and form finding of cable net for a large cable-rib tension antenna with flexible deployable structures. Eng Struct 199:109662

Maddio PD, Meschini A, Sinatra R et al (2019) An optimized form-finding method of an asymmetric large deployable reflector. Eng Struct 181:27–34

Meguro A, Harada S, Watanabe M (2003) Key technologies for high-accuracy large mesh antenna reflectors. Acta Astronaut 53(11):899–908

Min GR (1991) Satellite thermal control technology. Astronautics Press, Beijing (**In Chinese**)

Morterolle S, Maurin B, Quirant J et al (2012) Numerical form-finding of geotensoid tension truss for mesh reflector. Acta Astronaut 76:154–163

Nie R, He BY, Yan SZ et al (2019) Optimization design method for the cable network of mesh reflector antennas considering space thermal effects. Aerosp Sci Technol 94:105380

Orikasa T, Fujino Y, Miura A, et al (2013) A study of large reflector antenna mounted on communication satellite for satellite

Terrestrial mobile communication system. In: The 31st AIAA international communication satellite systems conference, Italy

Ruze J (1966) Antenna tolerance theory—A review. Proc IEEE 54(4):633–640

Sun ZH, Duan BY, Zhang YQ et al (2021) Influence and experiment of cable-net manufacturing errors on surface accuracy of mesh reflector antennas. Chin J Aeronaut. https://doi.org/10.1016/j.cja.2021.12.004

Tabata M, Natori MC (1996) Active shape control of a deployable space antenna reflector. J Intell Mater Syst Struct 7(2):235–240

Wang ZW, Li TJ, Cao YY (2013) Active shape adjustment of cable net structures with PZT actuators. Aerosp Sci Technol 26(1):160–168

Xun GB, Peng HJ, Wu SN et al (2018) Active shape adjustment of large cable-mesh reflectors using novel fast model predictive control. J Aerosp Eng 31(4):04018038

Yang GG, Duan BY, Du JL et al (2018b) Shape pre-adjustment of deployable mesh antennas considering space thermal loads. Proc IMechE Part G 232(g1):143–155

Yang GG, Duan BY, Zhang YQ et al (2016) Uniform-tension form-finding design for asymmetric cable-mesh deployable reflector antennas. Adv Mech Eng 8(10):1–7

Yang C, Hou XB, Wang L (2017) Thermal design, analysis and comparison on three concepts of space solar power satellite. Acta Astronaut 137:382–402

Yang GG, Tang AF, Yuan ZY et al (2020) Surface shape stability design of mesh reflector antennas considering space thermal effects. IEEE Access 8:89071–89083

Yang GG, Yang DW, Zhang YQ et al (2017) Form-finding design of cable-mesh reflector antennas with minimal length configuration. Aerosp Sci Technol 63:9–17

Yang DW, Zhang YQ, Yang GG et al (2018a) Least-squares minimization of boundary cable tension ratios for mesh reflectors. AIAA J 56(2):883–888

Zheng J, Chen H, Jiang C (2022) Robust topology optimization for structures under thermo-mechanical loadings considering hybrid uncertainties. Struct Multidisc Optim 65(1):1–16